Theoretical and Applied Mechanics Letters xxx (xxxx) xxx



Contents lists available at ScienceDirect

## Theoretical and Applied Mechanics Letters

journal homepage: www.elsevier.com/locate/taml



# Noise color influence on escape times in nonlinear oscillators - experimental and numerical results

Thomas Breunung\*, Balakumar Balachandran

Department of Mechanical Engineering, University of Maryland, College Park, MD 20742, United States

#### ARTICLE INFO

Article history:
Received 2 November 2022
Revised 28 November 2022
Accepted 30 November 2022

Keywords: Colored noise Non-Gaussian excitation Experiments Escape times

#### ABSTRACT

The interplay between noise and nonlinearites can lead to escape dynamics. Associated nonlinear phenomena have been observed in various applications ranging from climatology to biology and engineering. For reasons of computational ease, in most studies, Gaussian white noise is used. However, this noise model is not physical due to the associated infinite energy content. Here, the authors present extensive experimental investigations and numerical simulations conducted to examine the impact of noise color on escape times in nonlinear oscillators. With a careful parameterization of the numerical simulations, the authors are able to make quantitative comparisons with experimental results. Through the experiments and simulations, it is illustrated that the noise color can drastically influence escape times and escape probability.

© 2022 The Authors. Published by Elsevier Ltd on behalf of The Chinese Society of Theoretical and Applied Mechanics.

This is an open access article under the CC BY license (http://creativecommons.org/licenses/by/4.0/)

Noise induced escape is a fundamental phenomenon, which is due to the interplay between nonlinear and non-deterministic behavior. It has been used to explain change in climate trends [1], efficient neuronal communication in biology [2] and the occurrence of extreme events [3]. A prominent engineering application is bistable energy harvestering [4,5], wherein jumps between stable fixed points are utilized to generate power. More generally, the necessity of considering noise and nonlinearity simultaneously has been recognized, for example, in micro-electromechanical (MEMS) devices [6], energy harvesters [7], and offshore wind turbines [8]. However, in computational and experimental studies, nonphysical white noise is often employed and comparisons between experimental and computational results are usually limited to qualitative comparisons.

The most common noise model is Gaussian white noise, due to this noise model's simplicity and the associated sound theoretical basis. Indeed, various computational algorithms [9–11] and analytical results [12,13] have been obtained for the white noise case. However, this noise model has an infinite energy measure, and therefore, is nonphysical. Indeed, more realistic noise models for mechanical oscillators [14] and MEMS devices [15] as well as electrical circuits and metals [16] have been proposed. Consequently, in a few studies (e.g., Falsone and Elishakoff [17], Wein-

E-mail addresses: thomasbrn@umd.edu (T. Breunung), balab@umd.edu (B. Balachandran).

stein and Benaroya [18], Socha and Proppe [19], Li et al. [20], Jung and Hänggi [21]) non-Gaussian noise models have been considered. By and large, the results obtained are primarily of computational or theoretical nature and lack validation with experiments. Two notable exceptions are the studies [22,23], wherein electric circuits are employed to validate the associated theoretical findings. However, within these studies, only exponentially correlated noise has been considered and escape times have not been studied.

The effects of exponentially correlated noise have been studied in the context of stochastic resonance [24-28]. This classic phenomenon [29] occurs in bistable systems, where noise induced jumps between two equilibrium states are synchronized with an external excitation frequency. This mechanism has been utilized to explain complex dynamics in climatology [1], biology [2], and human sensation [30]. Amongst the investigations [24-28], there is agreement that the noise color alters, partially drastically, stochastic resonance in comparison to the white noise case. However, these studies are of computational character and they have not been experimentally validated. Notable exceptions are the experiments with electrical circuits reported in the studies [31,32]. Unfortunately, the results [31] on colored noise are only preliminary and no comparisons with simulation results have been made, and in Castro et al. [32], only qualitative comparisons with theoretical results have been reported.

Vibration energy harvesting is another active research area, wherein noise induced jumps have been exploited. Colored noise has received attention (e.g., Daqaq et al. [7], Zhu et al. [33],

https://doi.org/10.1016/j.taml.2022.100420

2095-0349/© 2022 The Authors, Published by Elsevier Ltd on behalf of The Chinese Society of Theoretical and Applied Mechanics. This is an open access article under the CC BY license (http://creativecommons.org/licenses/by/4.0/)

<sup>\*</sup> Corresponding author.

Theoretical and Applied Mechanics Letters xxx (xxxx) xxx

Tang et al. [34]), wherein it is employed to model a harvested broadband environmental source. While many studies are of either purely theoretical or experimental character, in a few studies [4,35], comparisons have been made between experimental and computational results. The main focus of these applications has been on the harvested power output. Hence, escape times have not been studied.

In a study from the authors' group [36], a series of investigations were initiated to utilize noise in mechanical systems. The effects of noise on the frequency response curve of a softening Duffing oscillator [37], the induced escape routes from chaotic attractors [38], and the generation and destruction of localization in coupled oscillator arrays [39] have been examined. In these studies, the corresponding researchers utilize noise as an inexpensive and omnipresent control input to steer mechanical systems into favorable operating conditions. Indeed, noise assisted response steering has been been proposed to suppress unwanted whirling motions in a rotor-stator system [40]. Despite this extensive body of work, only qualitative comparisons are made between experimental and computational results, and they are limited to white noise. Only in the investigation [41] on an circular oscillator array, the case of pink noise as an alternative colored, noise model has been considered. However, no experimental results were reported in this study.

In summary, experimental studies on noise induced escape are rare and the case of colored noise has not been studied. Moreover, quantitative comparisons of computational and experimental results are not available in the literature. This knowledge gap motivates the experimental campaign presented in this article. A bistable system is investigated here and the effects of different noise models on the noise induced escape times are recorded. Moreover, the experiments are accompanied with careful numerical studies, to show that the simulations can be used to accurately predict the escape times if the correct noise model is employed.

The experimental setup is shown in Fig. 1. An electrodynamic shaker (Brüel & Kær 4811) is used to excite the base plate and the attached metal cantilever. The shaker excitation is directed normal to the longitudinal axis of the cantilever structure. Hence, primarily bending modes are expected to be excited in this configuration. The associated vibrations are measured by using a strain gauge attached close to the cantilever base. Magnets are mounted at the cantilever free end and on the opposing end of the frame. These magnets have been arranged to attract each other, which results in a nonlinear relationship between the tip-displacement and the restoring force experienced by the cantilever. The control signals for the shaker, harmonic excitation with and without noise, are all generated by using LabVIEW software, which is also employed for data acquisition. The sampling frequency for all signals is 1.0 kHz.

By applying a purely harmonic forcing to the cantilever and recording the arising vibration amplitudes, the frequency response curve shown in Fig. 1b is constructed. For both sweeps, the frequency is changed by an increment of 0.02 Hz every thirty seconds. This slow sweep speed ensures that the observed response is close to a steady state. Indeed, increasing the frequency increment by a factor of five does not alter the response shown in Fig. 1b.

The amplitude of strain gauge signal shown in Fig. 1b can be related to motion in the first beam bending mode and the related tip displacement. The escape times, however, are independent of such transformations (i.e., from the strain gauge signal to the tip displacement). For this reason, the unconverted strain gauge signals are utilized in the following.

The hardening characteristic is clearly discernible in the frequency response shown in Fig. 1b. For frequencies between 38.5 Hz (jump-up frequency) and 39.8 Hz (jump-down frequency), two stable steady-state solutions are observed. The orbit with the larger amplitude is denoted as the high amplitude orbit and that with the low amplitude is denoted as the low amplitude orbit. If a

small noise input is added to the harmonic excitation, then jumps between the two coexisting steady-state solutions are initiated. Indeed, for autonomous (time-invariant, unforced) systems and purely white noise excitation, from the associated theory [42,43], it follows that for any arbitrarily small noise intensity, jumps between attractors occur. For non-autonomous (forced) mechanical systems, these jumps have also been well documented in simulations and experiments [37–41].

An experimentally observed escape is illustrated in Fig. 1c. Therein, the forcing frequency is 39.6 Hz and the vibrations are initiated in the high amplitude orbit. This initialization is experimentally achieved by gradually sweeping up from 38.0 Hz to 39.6 Hz. Once the value of 39.6 Hz is reached, the excitation frequency is kept constant and noise is added to the harmonic excitation signal. The time instance at which the noise is added is set to t=0 s. Initially, the response remains in the high amplitude orbit. However, after about 37 s, the response collapses to the low amplitude orbit and remains there for the duration of this experiment. The time duration that it takes for this collapse to occur is known as *escape time*.

In the experimental campaign to quantify the effects of different noise models on the escape time, the experiment shown in Fig. 1c is repeated (cf. Fig. 1b). First, the high amplitude response is realized by sweeping up from 38.0 Hz to 39.6 Hz. Then keeping the excitation frequency fixed, the noise perturbation is added to the harmonic shaker excitation. For an initial period, high amplitude oscillations are observed, before the response collapses to the low energy orbit<sup>1</sup> (cf. Fig. 1c). Then, the escape time is extracted from the recorded signal. For each noise model, the experiment is repeated 200 times to obtain accurate distributions of the escape times.

In the engineering and physics literature, noise models are often classified on the basis of the power spectral density shape (e.g., Saulson [14], Vig and Kim [15], Kogan [16]). The power spectral densities S(f) of the noise models considered in this study are of the form

$$S(f) \propto \frac{1}{f^{\alpha}},$$
 (1)

where f denotes the frequency and  $\alpha$  is a positive integer. The following noise models are considered in this article:

1. White noise ( $\alpha = 0$ ): As previously mentioned, white noise has a sound mathematical basis and is commonly used in computational studies. Therefore, it is included within this study as comparison. However, an ideal white noise signal has infinite energy measure, and hence, it cannot occur in reality. The utilization of white noise is often justified by either arguing that the power spectrum of the excitation is sufficiently flat over the frequency range of interest [44] or, equivalently, the correlation time is shorter than the system's characteristic time scale [28]. In the experiments, LabVIEW's random number generator is used to generate discrete samples, which are then converted into an analog signal for the shaker control signal. The sampling rate of 1.0 kHz limits the bandwidth of the experimentally realized noise to be at the Nyquist frequency of 500 Hz. Up to this frequency, the power spectrum of the generated noise is nearly constant.

<sup>&</sup>lt;sup>1</sup> Within this work, jumps from the high amplitude to the low amplitude orbit are observed in all cases within three minutes. Based on theory, one might be inclined to believe that trajectories might also jump up from the low amplitude orbit to the high amplitude orbit. However, these jumps were not observed for the investigated parameters. Noise induced jumps from the low amplitude orbit to the high amplitude orbit are generally more likely to be observed for the harmonic excitation frequencies that are closer to the jump up frequency (approx. 38.5 Hz in Fig. 1(b)).

Theoretical and Applied Mechanics Letters xxx (xxxx) xxx

JID: TAML [m5G;January 21, 2023;10:15]

(a)

T. Breunung and B. Balachandran

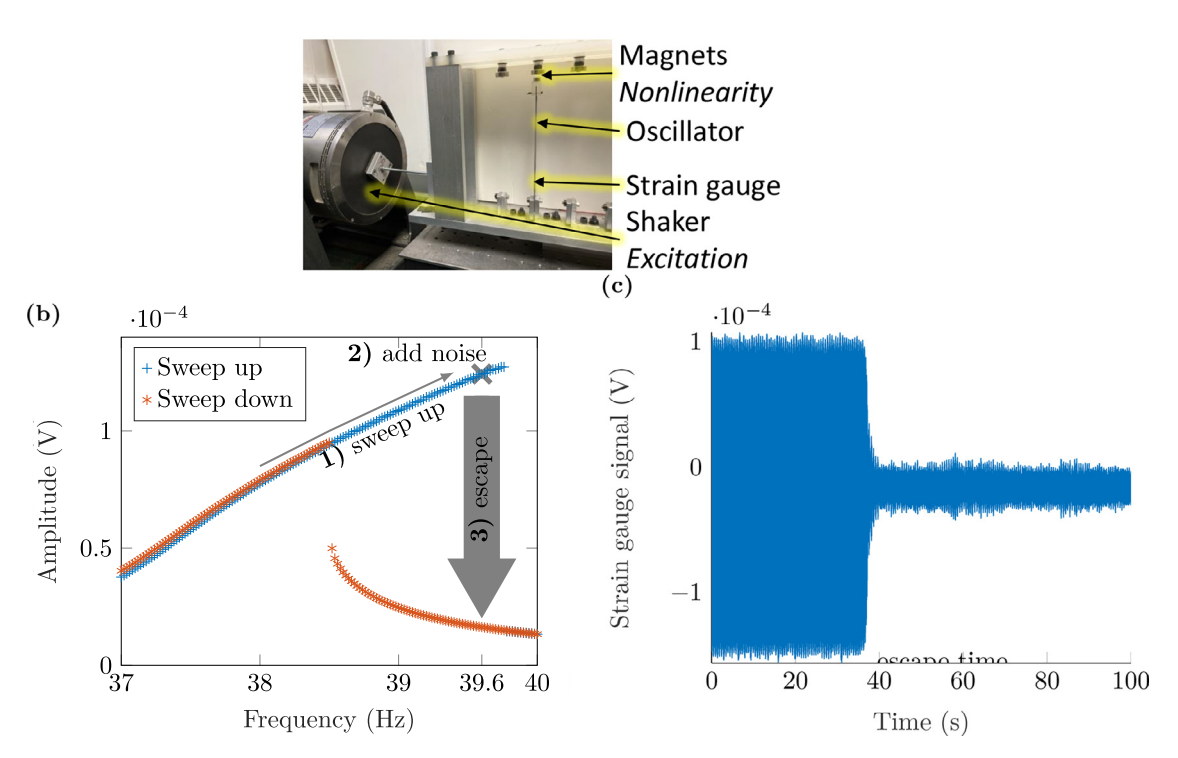


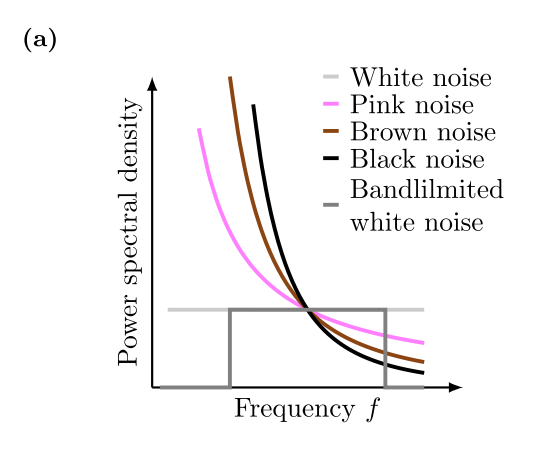
Fig. 1. (a) Experimental setup: The shaker is used to generate the external, harmonic and random excitation to the base of the metal cantilever. The resulting oscillations are measured with a strain gauge. A nonlinear restoring force follows from the magnets mounted at the cantilever tip and the fixed frame. (b) Measured cantilever response to sinusoidal excitation and experimental procedure: A sweep up is used to realize the high amplitude orbit. When the excitation frequency reaches 39.6 Hz, noise is added to the input and a noise induced escape is observed. (c) Time series of a strain gauge signal: The forcing frequency is 39.6 Hz and the response is initiated in the high energy orbit. After about 37.0 s an escape towards the low amplitude orbit is observed.

- 2. *Pink noise* ( $\alpha = 1$ ): Pink noise has been observed in various applications such as electrical circuits [45], metals [16], ocean waves [46], and human heart beats [47]. It is also referred to as Flicker noise or 1/f-noise, due to the shape of its power spectral density.
  - Technically, the power spectrum of the pink noise model approaches infinity as the frequency approaches zero  $(f \rightarrow 0)$  in Eq. (1)). Such excitations are, of course, impossible to realize experimentally. Moreover, the employed shaker has lower displacement and velocity limits for low frequencies. Hence, the idealized frequency spectrum of pink noise needs to be truncated. In this work, the generated pink noise is filtered with a Butterworth bandpass filter of tenth order with a passband between 10 Hz and 100 Hz before it is sent to the shaker as a control input.
- 3. Brownian noise ( $\alpha=2$ ): Brownian noise, herein abbreviated as brown noise, has been observed not only in MEMS devices [15] and optical mirrors for high precision measurements [48] but also in the height profile of road surfaces [49,50]. It can also be viewed as an exponential correlated noise where the correlation time is larger than the system's characteristic time scale (which can be the reciprocal of an eigenfrequency of the system under consideration).
  - Analogous to the pink noise case, only truncated versions of brown noise can be realized in experiments. Hence, the computer generated brown noise is filtered with the same filter as the pink noise (tenth order Butterworth bandpass with a passband between 10 Hz and 100 Hz) before it is added to the sinusoidal shaker control input.
- 4. Black noise ( $\alpha = 3$ ): Black noise can, for example, be traced in geophysical time series [51,52]. In general, geophysical time

- series can have considerable long-range statistical dependencies [53] and hence, they feature a power spectrum decaying with exponents larger than two [52]. Black noise has a significant energy content at low frequencies and only minimal amplitudes at high frequencies.
- The demands on the experimental setup for low frequencies, in particular, the shaker, are even more increased for black noise compared to the pink and brown noise cases. In the current experimental setup, considerable filtering needs to be applied to experimentally realize black noise. This filtering significantly distorts black noise, especially, in the dynamic range of interest (10–100 Hz). Hence, no experiments with black noise are conducted and it is only utilized within the simulations for comparison.
- 5. Bandlimited white noise: Bandlimited white noise can be a close approximation of many physical processes [54]. It can be obtained by applying a bandpass filter to an ideal white noise signal. Bandlimited white noise is also included to test the hypothesis that a flat spectrum can be approximated with a broadband white noise signal.
  - In the experiments, white noise is filtered to generate bandlimited white noise. To this end, the same filter which is also utilized to filter pink and brown noise is employed; that is, a tenth order Butterworth bandpass with a passband between 10 Hz and 100 Hz.

The idealized and experimentally realized noise models are shown in Fig. 2. Moreover, all noise models have been scaled to have the same power spectral density at the system's eigenfrequency of 37.5 Hz (cf. Fig. 2b). This scaling ensures comparability between the noise models. Additionally, each noise model has approximately the same energy measure in the frequency band of

Theoretical and Applied Mechanics Letters xxx (xxxx) xxx



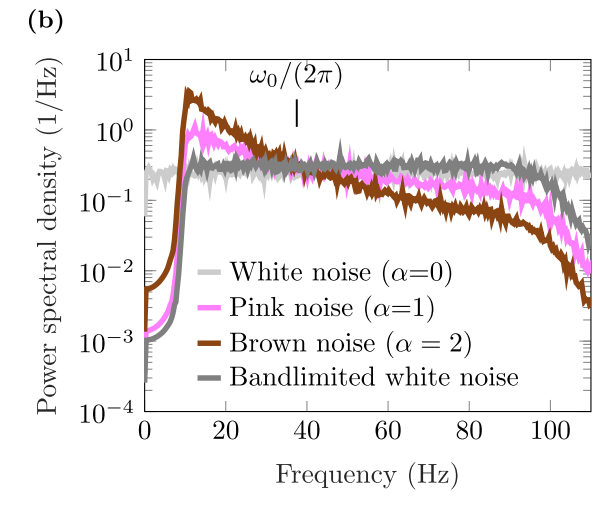
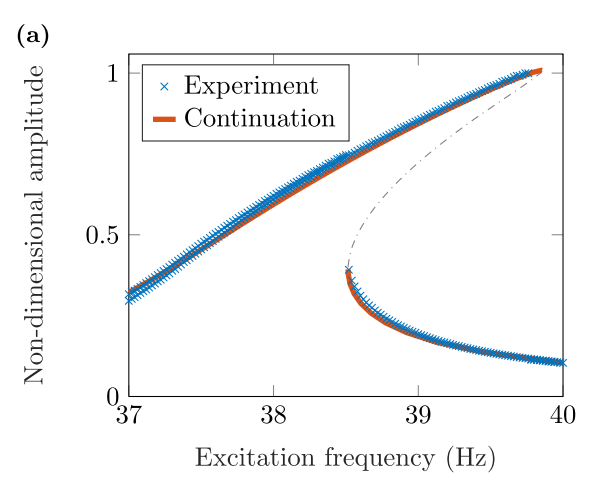
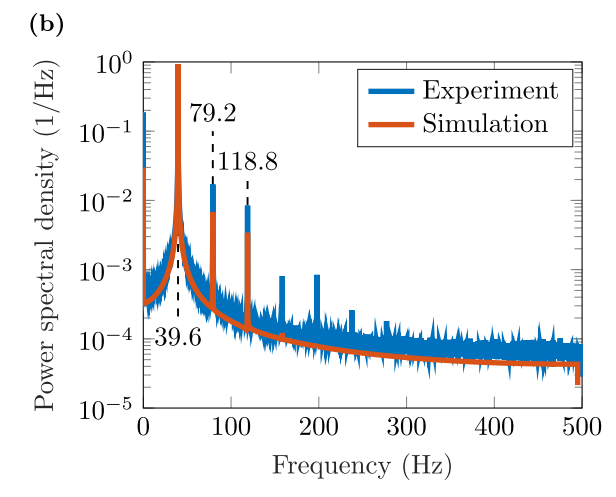


Fig. 2. Power spectral density of the considered noise models. (a) Idealized power spectral density. (b) Experimentally realized power spectral densities.





**Fig. 3.** Deterministic system identification for purely harmonic excitation. (a) Fitted and measured frequency response curve. (b) Response frequency spectrum for the high amplitude orbit at  $f = \Omega/(2\pi) = 39.6$  Hz.

interest. Therein, the energy measure is defined as the sum of the absolute values of the Fourier coefficients within the frequency interval between 10 Hz and 100 Hz.

The experiments discussed in the preceding sections are accompanied by simulations. To this end, a simulation model is derived and parameterized as discussed. The numerical techniques used to simulate the dynamical systems subject to colored noise are illustrated.

To facilitate simulations, the cantilever vibrations need to be modeled. In previous studies [37–39,55] Duffing's equation has been utilized for modeling such structures in similar experiments. Such a model can be theoretically justified by a Galerkin projection of an underlying partial differential equation governing the vibrations of the beam (modeled as a continuum) [55,56]. The frequency content of the measurements taken to obtain the frequency response curve (cf. Fig. 1b), however, reveals a significant second harmonic (cf. Fig. 3b), which does not arise in the solution of the sinusoidal forced Duffing equation. To account for the second harmonic, Duffing's equation is extended by including a quadratic term yielding

$$\ddot{q} + c\dot{q} + \omega_0^2 q + \kappa_2 q^2 + \kappa_3 q^3 = a \sin(\Omega t) + \sigma n(t), \tag{2}$$

where  $\omega_0$  denotes the linear natural frequency, c is the damping coefficient,  $\kappa_3$  is the cubic spring coefficient, and  $\kappa_2$  is the quadratic spring coefficient. Quadratic coefficients are classically

related to asymmetries. In the experiment shown in Fig. 1a, asymmetries arise from, for example, the asymmetric clamping and the non-perfectly centered magnets. Furthermore, electrodynamic shakers are also known to introduce higher, especially, second, harmonics [57]. The forcing on the right hand side of Eq. (2) consists of a sinusoidal term with amplitude a and angular frequency  $\Omega$  and the noise term  $\sigma n(t)$ . The parameter  $\sigma$  denotes the intensity of the noise, whereas n(t) follows from the noise models introduced.

The external forcing frequency, generated by the shaker, is known, whereas the remaining coefficients,  $\omega_0$ , c,  $\kappa_2$ ,  $\kappa_3$ , a, and  $\sigma$  are unknown. Hence, they need to be identified. To facilitate a better fit, the measured amplitude values are normalized and nondimensionalized by introducing

$$\eta = 12.732 \text{ mV}, \qquad \tilde{q} := \frac{q}{n}.$$

The factor  $\eta$  was selected to be the maximal amplitude of the sweep shown in Fig. 1b. In the following, the equation

$$\ddot{\tilde{q}} + \hat{c}\dot{\tilde{q}} + \hat{\omega}_0^2 \tilde{q} + \hat{\kappa}_2 \tilde{q}^2 + \hat{\kappa}_3 \tilde{q}^3 = \hat{a}\sin(\Omega t) + \hat{\sigma}n(t), \tag{3}$$

governing the non-dimensional amplitude  $\tilde{q}$  is considered. Eq. (3) is the normalized and non-dimensional equivalent of Eq. (2) is considered.

The parameters in Eq. (3) are first fitted for a purely harmonic excitation ( $\sigma = 0$ ). To this end, a computed frequency re-

Theoretical and Applied Mechanics Letters xxx (xxxx) xxx

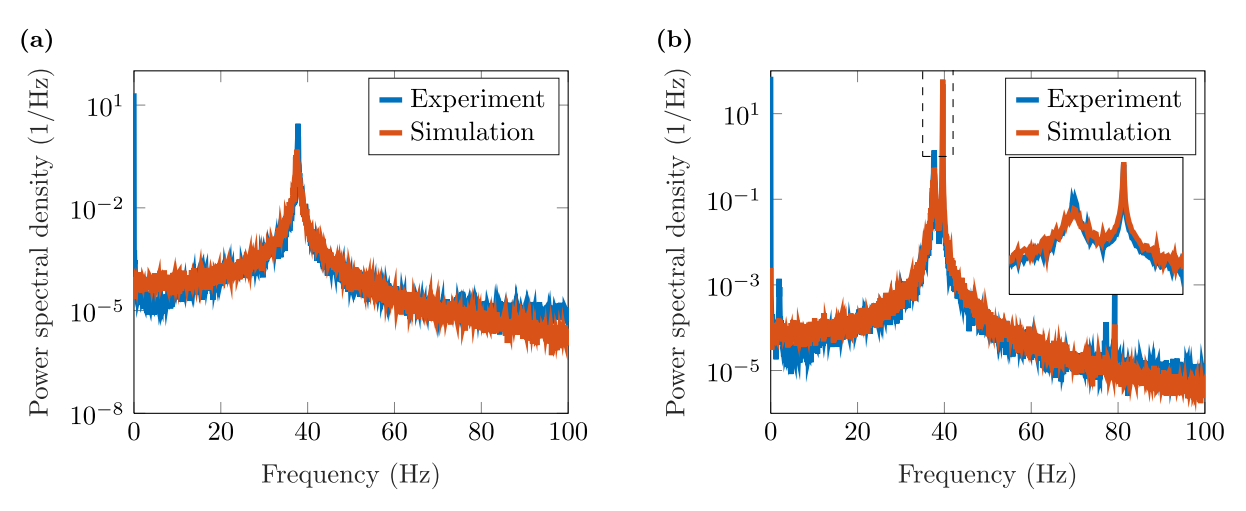


Fig. 4. Identification of the noise intensity. (a) White noise excitation only. (b) Simultaneous harmonic and white noise excitation.

sponse curve is fitted to the measured frequency response curve shown in Fig. 1(b). First, a curve fit of an analytic frequency response curve obtained via a perturbation scheme [56] to the measured data is obtained. Within this step, the quadratic coefficient  $\hat{\kappa}_2 = 0$  is set to zero, since an infinite number of combinations of quadratic and cubic coefficients ( $\kappa_2$  and  $\hat{\kappa}_3$ ) yield the same frequency response curve [56]. The curve fitting leads to a nonlinear optimization problem, which is solved using Matlab's Isqnonlin routine.

The parameters obtained from the perturbation result are successively corrected through numerical computations of the frequency response curve. To this end, the frequency response is computed with numerical continuation package coco [58], and then, the parameters are manually adjusted to obtain a close match. Herein, only the damping value needs to be adjusted, whereas that natural frequency  $\hat{\omega}_0$ , the cubic coefficient  $\hat{\kappa}_3$ , and the forcing amplitude  $\hat{a}$  were retained from the nonlinear curve fit. As shown in Fig. 3a, the computed frequency response curve matches closely with the measured response curve.

Finally, the quadratic coefficient  $(\hat{\kappa}_2)$  is obtained by matching the second harmonic in the frequency spectrum for a forcing frequency of 39.6 Hz (cf. Fig. 3b). While the quadratic coefficient  $\hat{\kappa}_2$  is adjusted, the cubic coefficient  $\hat{\kappa}_3$  is changed accordingly such that the frequency response curve (cf. Fig. 3a) is not altered. The identification procedure yields the parameters

$$\begin{split} \hat{\omega}_0/(2\pi) &= 37.54 \text{ Hz}, \quad \hat{c} = 3.11 \text{ s}^{-1}, \quad \hat{\kappa}_2 = 4000 \text{ s}^{-2}, \\ \hat{\kappa}_3 &= 8775.85 \text{ s}^{-2}, \qquad \hat{a} = 781.21 \text{ s}^{-2}. \end{split}$$

To obtain the noise intensity  $\hat{\sigma}$ , the cantilever is excited with noise only, and then, by applying harmonic and random excitation simultaneously. The power spectrum of the measured and computed response are compared. Subsequently, the noise intensity  $\hat{\sigma}$  is adjusted until the both power spectra, experimental and simulated, match in the frequency range between 20 Hz and 80 Hz. For  $\hat{\sigma}=13.98$ , the response spectra obtained with purely white noise excitation and to simultaneous harmonic and white noise excitation match closely, as shown in Fig. 4. For the other noise models, a similar close fit between simulations and experiments is noted.

To compute escape times for system (Eq. (3)), the associated responses to stochastic excitations need to be calculated. To this end, numerical time integration is employed. In this context, it is noted that computational routines for stochastic dynamical systems have been primarily developed for Gaussian white noise [9–11]. Since the noise models can be obtained by filtering white noise, numerical integrators developed for Gaussian white noise can be utilized for the colored noise models. To this end, the fil-

ter is written as a dynamical system. Filters are most commonly designed as discrete time systems of the form

$$\mathbf{z}_{n+1} = \mathbf{A}_d \mathbf{z}_n + \mathbf{B}_d W_n, \quad n(t_n) = \mathbf{C}_d \mathbf{z}_n + D_d W_n. \tag{4}$$

Therein, the variable  $\mathbf{z} \in \mathbb{R}^{N_f}$  is the state of the filter,the integer  $N_f$  is the dimension of the filter state, and W is the one dimensional Wiener process. The dimensions of the matrices and vectors are as follows:  $\mathbf{A}_d \in \mathbb{R}^{N_f \times N_f}$ ,  $\mathbf{B}_d \in \mathbb{R}^{N_f}$ , and  $\mathbf{C}_d \in \mathbb{R}^{1 \times N_f}$ . These matrices and  $D_d$  need to be determined such that the noise term  $n(t_n)$  resembles the noise models presented, and can be employed in Eq. (3). For the each noise model listed in previous discussion, a different filter is employed. The selected filters and their coefficients, which are stored in the matrices  $\mathbf{A}_d$ ,  $\mathbf{B}_d$ ,  $\mathbf{C}_d$  and  $\mathbf{D}_d$ , are listed in Ref. a.

To incorporate the filter Eq. (4) into the oscillator model Eqs. (3) and (4) needs to be reformulated in continuous time. For this purpose, the state  $\tilde{\mathbf{z}}_n := \left[\mathbf{z}_n^{\mathsf{T}}, n(t_{n-1})\right]^{\mathsf{T}}$  is introduced, which yields the more compact form

$$\tilde{\mathbf{z}}_{n+1} = \begin{bmatrix} \mathbf{A}_d & \mathbf{0} \\ \mathbf{C}_d & 0 \end{bmatrix} \tilde{\mathbf{z}}_n + \begin{bmatrix} \mathbf{B}_d \\ D_d \end{bmatrix} W_n = \tilde{\mathbf{A}}_d \tilde{\mathbf{z}}_n + \tilde{\mathbf{B}}_d W_n.$$
 (5)

The discrete time system (Eq. (5)) can be viewed as an Euler–Maruyama discretization of a continuous time stochastic process of the form

$$d\mathbf{z} = \mathbf{A}_{c}\mathbf{z}dt + \mathbf{B}_{c}dW \overset{\text{Euler-Maruyama}}{\Rightarrow} \mathbf{z}_{n+1} = (\mathbf{I} + \mathbf{A}_{c}\tau)\mathbf{z}_{n} + \sqrt{\tau}\mathbf{B}_{c}W_{n},$$
(6)

where  $\tau$  is the time between two discrete time instances. For small enough time steps  $\tau$ , the sample paths of the Euler Maruyama discretization (Eq. (6)) converge to the sample paths of the stochastic differential equation in continuous time in the strong sense [11]. Hence, the discrete filter Eq. (5) can be approximated by the continuous stochastic differential Eq. (6) by setting

$$\mathbf{A}_{c} := \frac{1}{\tau} (\tilde{\mathbf{A}}_{d} - \mathbf{I}), \qquad \mathbf{B}_{c} := \frac{1}{\sqrt{\tau}} \tilde{\mathbf{B}}_{d}. \tag{7}$$

The noise  $n(t_n)$  is included as the last entry of the state  $\tilde{\mathbf{z}}_{n+1}$ . Since the state  $\mathbf{z}$  is the continuous time equivalent to the state  $\tilde{\mathbf{z}}_{n+1}$ , the last entry of  $\mathbf{z}$  yields the continuous time noise process n(t), and this can be extracted as follows

$$n(t) = [0, 0, ..., 1]\mathbf{z} = \mathbf{C}_c \mathbf{z}.$$

This equation can be utilized to simulate system (Eq. (3)). To this end, system (Eq. (3)) can be written in first order form, by introducing the state  $\mathbf{x} := \left[\tilde{q}, \dot{\tilde{q}}, \mathbf{z}^{\top}\right]^{\top}$  which in differential form yields

Theoretical and Applied Mechanics Letters xxx (xxxx) xxx

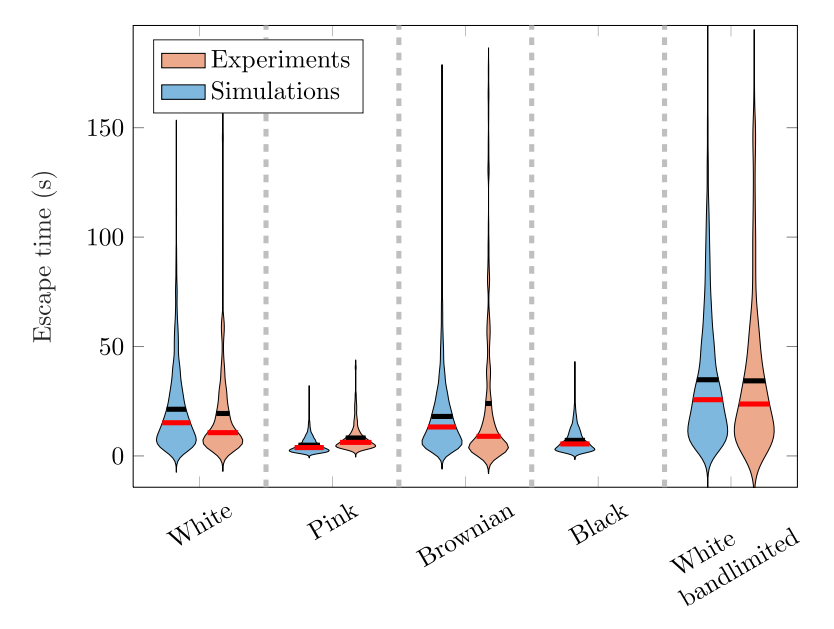


Fig. 5. Experimentally and numerically obtained probability densities of the escape times for the different noise models. The black line indicates the mean, and the red lines indicate the median. Black noise is not realizable in the experimental set up. Hence, no experimental results for this noise model are included.

$$d\mathbf{x} = d \begin{bmatrix} \tilde{q} \\ \dot{\tilde{q}} \\ \mathbf{z} \end{bmatrix} = \begin{bmatrix} -\hat{c}\dot{\tilde{q}} - \hat{\omega}_0^2 \tilde{q} - \hat{\kappa}_2 \tilde{q}^2 - \hat{\kappa}_3 \tilde{q}^3 + \hat{a}\sin(\Omega t) + \hat{\sigma} \mathbf{C}_c \mathbf{z} \\ \mathbf{A}_c \mathbf{z} \end{bmatrix}$$
$$dt + \begin{bmatrix} 0 \\ 0 \\ \mathbf{B}_c \end{bmatrix} dW = \mathbf{f}(\mathbf{x}, t) dt + \mathbf{B} dW. \tag{8}$$

Equation (8) is in the form of a stochastic differential equation excited by Gaussian white noise. This means that numerical routines developed for this setting become available. Here, the efficient stochastic integrator from the authors' prior work [59] is employed. This integration routine has been shown to be efficient for similar systems and yield an computational speedup of up to two orders of magnitude compared to the standard Euler–Maruyama scheme. This efficiency allows to compute the escape time of 2000 samples for each noise model.

From each simulation or experimental run, an escape time is obtained (cf. Fig. 1c for an illustration). Due to the stochasticity present, the escape time is a random variable with an underlying distribution for each noise model. The numerically and experimentally obtained distributions of the escape times are shown in Fig. 5. The probability densities are visualized in a violin plot.<sup>2,3</sup> The computationally and experimentally obtained probability densities match very well for each noise model. The mean square error between the computed and experimental probabilities is about 2% for the pink noise model, whereas for the other noise models, the error is below 0.2%.

For all distributions shown in Fig. 5, the mean escape time is larger than the median escape time which is, in turn, larger than the most probable escape time (= mode). This observation indicates a positive skew of the underlying distributions. Therefore, the escape time distributions are necessarily non-Gaussian. This char-

acteristic can be related to two factors. First, the escape time is strictly positive. Moreover, the heavy tails can be explained by observing that even for long times there is a non-zero probability that the net effect of the noise on the dynamics of the deterministic system is negligible and hence no escape is observable. These two facts give rise to the positive skew and heavy tails of the escape time distributions shown in Fig. 5.

A more detailed picture of the mean escape times is provided in Fig. 6a. Therein, the effects of the different noise models are clearly discernible. Compared to white noise, with pink noise, the mean escape time is decreased by a factor of about three. A similar observation is made for the black noise case. Interestingly, the mean escape times for brown noise is approximately the same as that for white noise. Thus, no distinct trend for the mean escape times and the coefficient  $\alpha$  describing the power spectrum of the noise model (cf. Eq. (1)) is observed. With increasing  $\alpha$ , the mean escape times first drops (the pink noise case), then increases (brown noise), and drops again (black noise). In particular, the drastic reduction of the mean escape times with pink noise stands out.

Bandlimiting white noise clearly has an influence on the mean escape time. For the chosen parameters, the mean escape time increases for bandlimited white noise by about 50% compared to the band-unlimited case. It is noted that the passband of the bandlimited white noise is between 10 Hz and 100 Hz and the power spectrum is essentially flat in the vicinity of the natural frequency (cf. Fig. 2b). Hence, one might be inclined to argue that the bandlimited process can be replaced with white noise. The experiments and simulations shown in Figs. 5 and 6a, however, indicate that such an approximation is not always justified. Thus, the validity of approximating a bandlimited process by white noise needs carefully consideration in practice.

The escape probability, shown in Fig. 6b, confirms the trend observed for the mean escape times. The escape probability for pink and black noise is the highest, while it is similar for brown noise and white noise and it is the lowest for the bandlimited white noise. This means that for a fixed time, an escape in the system perturbed by pink or black noise is more likely than for either white or brown noise. On the other hand, for bandlimited noise, an escape is less likely compared to the white noise case.

In this work, the authors have presented experimental and numerical results on the escape times in a nonlinear oscillator for

<sup>&</sup>lt;sup>2</sup> The thickness of the violins indicate the probability density. Therein, a continuous probability density function is estimated from a finite number of samples by utilizing kernel smootheners. The underlying assumption is that a normal distribution with a certain bandwidth is induced by each sample. Compared to histograms, violin plots do not depend on a selected bin width. Moreover, violin plots can reveal multimodal distributions, which are not easily discernible from, for example, box-plots.

<sup>&</sup>lt;sup>3</sup> The authors are thankful to Holger Hoffmann for making his code available [60].

Theoretical and Applied Mechanics Letters xxx (xxxx) xxx

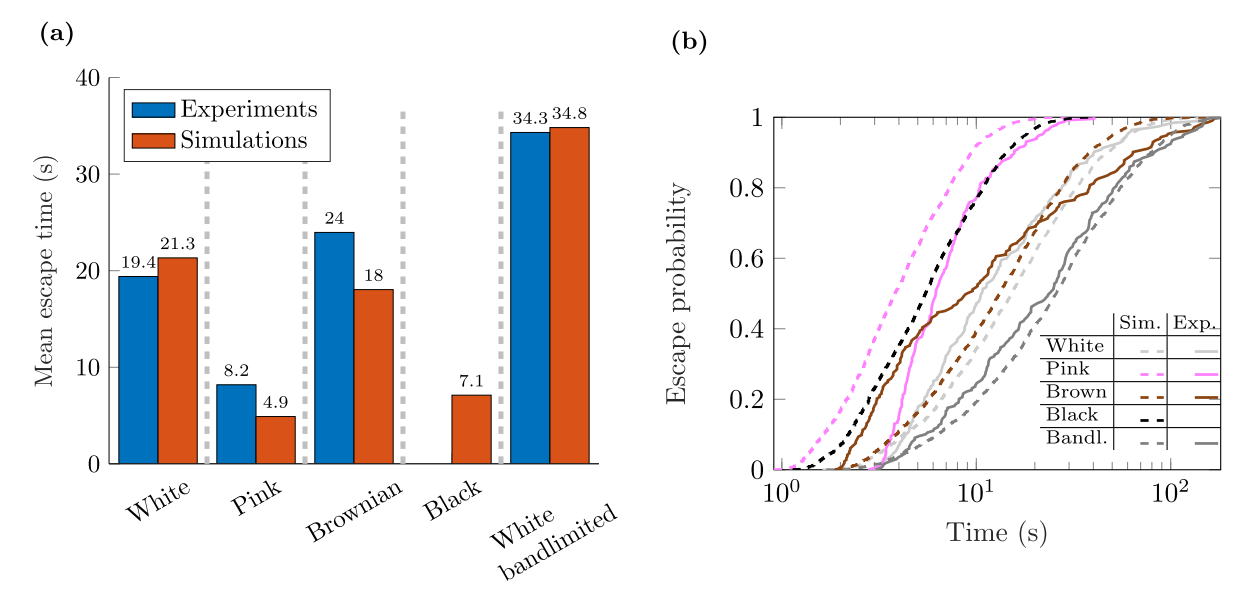


Fig. 6. (a) Mean escape time for the different noise models<sup>a</sup>. (b) Escape probability for the different noise models<sup>a</sup>. <sup>a</sup>Black noise is not realizable in the experimental set up. Hence, no experimental results for this noise model are included.

different noise colors. The experimental arrangement consists of an electrodynamical shaker exciting a cantilever structure. Magnets attached to the tip of the cantilever and the fixed frame induce a nonlinear force-deflection curve and the frequency response has a hardening behavior with a bistable region (cf. Fig. 1b). Within this multistability region, noise induced jumps between the coexisting attractors have been observed. In particular, the durations of transitions from the high amplitude orbit to the low amplitude orbit for different noise models have been recorded. For each of the four experimentally realizable noise models, the escape time of 200 samples has been measured.

To enable the simulations, the experimental arrangement has been modeled as a nonlinear oscillator with a spring force featuring quadratic and cubic terms. These parameters as well as the noise intensity have been identified from experimental data. To utilize simulation tools designed for Gaussian white noise to simulate colored noise excitations, the filter equations are incorporated into the dynamical system. Then, the escape times for 2000 samples can be computed with the efficient stochastic integration routine [59].

The obtained results show a compelling agreement between the simulation and experimental results. This match shows that given a careful experimentation and correct parameterization of the models not only qualitative but also quantitative agreements can be obtained. Moreover, the experiments and simulations show that different noise models can have a drastic impact on the escape characteristics. An escape for pink noise is significantly more likely and this happens faster on average than with white noise. The same observation is made for black noise. The escape times and probabilities for brown noise are approximately comparable to those for the white noise case. When bandlimited noise is employed, the mean escape time increases and the respective escape probability decreases.

Especially noticeable is the reduced escape time for pink noise. In the future, it would be of great interest to conduct more parameter studies to uncover the universality of this observation. Given the presence of pink noise in many applications ranging from electronics, solid state physics to environmental science, such a study could have a broad impact. Similarly, for the other noise models, further parameter studies could reveal the universality of the observations detailed here.

Moreover, the bandlimitation of the white noise has a clear impact on the escape characteristics in the experiments conducted here. Hence, approximations of bandlimited processes by band-unlimited white noise, an engineering best practice [54], needs careful consideration. It would be desirable to carry out theoretical and experimental investigations into when such an approximation can be justified.

Although the impact of the different noise models on the escape characteristics is clearly noticeable (e.g., cf. Fig. 6a), no general trend between the noise color (coefficient  $\alpha$  in Eq. (1)) and the escape characteristics has been observed. It is envisioned that the experimental and computational investigations can be continued, to either confirm the absence of a clear trend or uncover a hidden relationship.

Within this article, the impacts of five different noise models on the escape times have been investigated and compared. The noise models have been selected based on engineering relevance. Due to the omnipresence of noise in any realistic setting many other models can be considered. Future investigations could, for example, include stochastic turbulence models such as Dryden's model [61], Lévy walks for biological systems [62,63], fractional Brownian motion [64] or multiplicative (state-dependent) noise for microelectromechanical (MEMS) devices [15].

While the escape times for system (2) have been obtained by numerical simulations in this article, it would be desirable to derive them theoretically in the future. However, to the best of the author's knowledge no result is readily available to compute the escape times of system (2). Often escape times calculations are based on the large deviation theory prominently summarized in Ref. [43]. Furthermore, these results rely on very restrictive assumptions, most severely they require a non-singularity condition on the stochastic diffusion terms (matrix **B** in Eq. (8)). However, this condition is not satisfied for mechanical systems.<sup>4</sup>

### **Declaration of Competing Interest**

Authors declare that they have no conflict of interest.

<sup>&</sup>lt;sup>4</sup> It is required that the diffusion matrix  $\mathbf{D} = \mathbf{B}\mathbf{B}^{\top}$  is non-singular. Since the noise terms do not force the velocity coordinates in Eq. (8), this requirement is not satisfied for system (2) and more general mechanical systems.

#### Acknowledgments

The authors gratefully acknowledge the support of the National Science Foundation through Grant no. CMMI 1760366 and the associated data science supplements. A preliminary report of this work has been presented and discussed at the ASME 2022 International Design Engineering Technical Conference & Computer and Information in Engineering conference (IDETC/CIE 2022). Moreover, T.B. is thankful to Lautaro Clienti for ongoing discussions throughout this work.

#### Appendix A

Filter coefficients

In this appendix, the filters generating colored noise are listed. The time step  $\tau$  to convert all discrete time system (Eq. (4)) to a continuous time domain (cf. Eq. (7)) is set to  $\tau = 0.001$  s.

The discrete time filter from Ref. [65] is utilized to generate pink noise.<sup>5</sup> The state space representation (Eq. (4)) is given by

$$\mathbf{A}_{d}^{p} = \text{diag}([0.99886, 0.99332, 0.96900, 0.86650, 0.55000, -0.7616]), \qquad \mathbf{B}_{d}^{p} = 0.2641 \begin{bmatrix} 0.0555179 \\ 0.0750759 \\ 0.1538520 \\ 0.3104856 \\ 0.5329522 \\ 0.0168980 \end{bmatrix}, \tag{A1}$$

$$\mathbf{C}_d^p = [1, 1, 1, 1, 1, 1], \qquad D_d^p = 0.6521,$$

where the notation  $diag(\mathbf{v})$  is used to denote a diagonal matrix with the entries taken from the vector  $\mathbf{v}$ .

To generate brown noise, a discrete time implementation of a first order low-pass filter is employed. Therein, the cut-off frequency needs to be set sufficiently low, so that the power spectrum decays quadratically over the frequency band of interest. To this end, the cut-off frequency  $\omega_c$  was set to  $0.2\pi$  rad/s. After setting the sampling time to  $\tau = 0.001$  s, the following coefficients are obtained:

$$A_d^b = \frac{1}{1 + \tau \omega_c} = 0.9994, \qquad B_d^b = 319.7076 \frac{\tau \omega_c}{1 + \tau \omega_c} = 0.2008, \qquad C_d^b = 1, \qquad D_d^b = 0. \tag{A2}$$

To generate black noise, pink noise is filtered with a first order low-pass filter. First, the filter coefficients Eqs. (A1) and (A2) are converted via Eq. (7) to yield their respective continuous time equivalents  $\mathbf{A}_c^p$ ,  $\mathbf{B}_c^p$ , and  $\mathbf{C}_c^p$  for the pink noise case, respectively  $\mathbf{A}_c^b$ ,  $\mathbf{B}_c^b$ , and  $\mathbf{C}_c^b$  for the first order low-pass filter. Then, these matrices are combined to have

$$\mathbf{A}_{c}^{bl} := \begin{bmatrix} \mathbf{A}_{c}^{p} & \mathbf{0} \\ \mathbf{B}_{c}^{b} \mathbf{C}_{c}^{p} & \mathbf{A}_{c}^{b} \end{bmatrix}, \qquad \mathbf{B}_{c}^{bl} := \begin{bmatrix} \mathbf{B}_{c}^{p} \\ \mathbf{0} \end{bmatrix}, \qquad \mathbf{C}_{c}^{bl} := [\mathbf{0}, 1]. \tag{A3}$$

A bandpass filter is employed to generate bandlimited white noise. This filter is constructed by using designfilt, an automated filter design tool of Matlab's Signal Processing toolbox. An infinite impulse response<sup>6</sup> bandpass filter of order eight with a passband between 10 Hz and 100 Hz is selected. From the Matlab routine, the following coefficients are obtained:

$$\mathbf{A}_{d} = \begin{bmatrix} 1.3768 & -0.6873 & 0 & 0 & 0 & 0 & 0 & 0 \\ 1.0000 & 0 & 0 & 0 & 0 & 0 & 0 & 0 \\ 0.3499 & -0.4288 & 1.9557 & -0.9597 & 0 & 0 & 0 & 0 \\ 0 & 0 & 1.0000 & 0 & 0 & 0 & 0 & 0 \\ 0.0798 & -0.0978 & 0.4462 & -0.4472 & 1.8711 & -0.8764 & 0 & 0 \\ 0 & 0 & 0 & 0 & 1.0000 & 0 & 0 & 0 \\ 0.0182 & -0.0223 & 0.1018 & -0.1020 & 0.4269 & -0.4281 & 1.1952 & -0.3854 \\ 0 & 0 & 0 & 0 & 0 & 0 & 1.0000 & 0 \end{bmatrix}, \qquad \mathbf{B}_{d} = \begin{bmatrix} 0.2541 \\ 0 \\ 0.0646 \\ 0 \\ 0.0147 \\ 0 \\ 0.0034 \\ 0 \end{bmatrix}, \tag{A4}$$

To verify the performance of the constructed filter, each filter is excited by white noise and the power spectrum of the response is computed. These spectra are shown in Fig. A1. By construction, each filter is found to give rise to a different response power spectrum shape.

 $<sup>^{5}</sup>$  The authors are thankful to Paul Kellet for making his developed filter publicly available [65].

<sup>&</sup>lt;sup>6</sup> The current state of infinite impulse response filters (IIR filter) is a linear combination of the excitation at the previous time steps as well as the previous filter outputs. The feedback of the previous filter outputs into the current state gives rise to poles and hence the possibility for infinite impulse response as well as instability. On the contrary, finite impulse response filters (FIR filters) do not allow for feedback of the previous filter output and, hence, they have a finite impulse response.

Theoretical and Applied Mechanics Letters xxx (xxxx) xxx

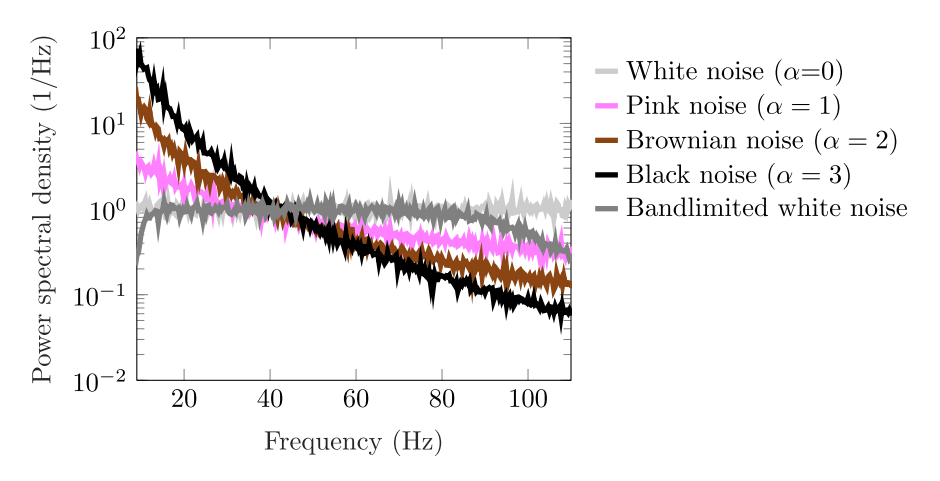


Fig. A1. Power spectral density of the filter response to white noise excitation.

#### References

- [1] R. Benzi, G. Parisi, A. Sutera, et al., Stochastic resonance in climatic change, Tellus 34 (1982) 10-16.
- [2] J.K. Douglass, L. Wilkens, E. Pantazelou, et al., Noise enhancement of information transfer in crayfish mechanoreceptors by stochastic resonance, Nature 365 (1993)
- [3] M. Farazmand, T.P. Sapsis, Extreme events: mechanisms and prediction, Appl. Mech. Rev. 71 (2019) 050801, doi:10.1115/1.4042065.
- [4] F. Cottone, H. Vocca, L. Gammaitoni, Nonlinear energy harvesting, Phys. Rev. Lett. 102 (2009) 080601.
- [5] R.L. Harne, K. Wang, A review of the recent research on vibration energy harvesting via bistable systems, Smart Mater. Struct. 22 (2013) 023001.
- [6] M. Pardo, L. Sorenson, F. Ayazi, An empirical phase-noise model for MEMS oscillators operating in nonlinear regime, IEEE Trans. Circuits Syst. I 59 (2012) 979-988.
- [7] M.F. Daqaq, R. Masana, A. Erturk, et al., On the role of nonlinearities in vibratory energy harvesting: A critical review and discussion, Appl. Mech. Rev. 66 (2014).
- [8] A. Banerjee, T. Chakraborty, V. Matsagar, et al., Dynamic analysis of an offshore wind turbine under random wind and wave excitation with soil-structure interaction and blade tower coupling, Soil Dyn. Earthq. Eng. 125 (2019) 105699.
- [9] D. Kannan, V. Lakshmikantham, Handbook of Stochastic Analysis and Applications, CRC Press, 2001.
- [10] E. Platen, An introduction to numerical methods for stochastic differential equations, Acta Numer. 8 (1999) 197–246.
- [11] P.E. Kloeden, E. Platen, Numerical Solution of Stochastic Differential Equations, Applications of Mathematics, vol 23, Springer, Berlin, 1999.
- [12] C. Soize, The Fokker–Planck Equation for Stochastic Dynamical Systems and its Explicit Steady State Solutions, vol. 17, World Scientific, 1994.
- [13] T. Caughey, Nonlinear theory of random vibrations, in: Advances in Applied Mechanics, vol. 11, Elsevier, 1971, pp. 209-253.
- [14] P.R. Saulson, Thermal noise in mechanical experiments, Phys. Rev. D 42 (1990) 2437.
- [15] J.R. Vig, Y. Kim, Noise in microelectromechanical system resonators, IEEE Trans. Ultrason., Ferroelectr., Freq. Control 46 (1999) 1558-1565.
- [16] S. Kogan, Electronic Noise and Fluctuations in Solids, Cambridge University Press, Cambridge, 1996
- [17] G. Falsone, I. Elishakoff, Modified stochastic linearization technique for colored noise excitation of duffing oscillator, Int. J. Non-linear Mech. 29 (1994) 65–69.
- [18] E.M. Weinstein, H. Benaroya, The van Kampen expansion for the Fokker-Planckequation of a duffing oscillator excited by colored noise, J. Stat. Phys. 77 (1994) 681-690.
- [19] L. Socha, C. Proppe, Control of the duffing oscillator under non-gaussian external excitation, Eur. J. Mech. A/Solids 21 (2002) 1069-1082
- [20] C. Li, W. Da-Jin, K. Sheng-Zhi, Bistable kinetic model driven by correlated noises: unified colored-noise approximation, Phys. Rev. E 52 (1995) 3228.
- [21] P. Jung, P. Hănggi, Dynamical systems: a unified colored-noise approximation, Phys. Rev. A 35 (1987) 4464.
- [22] P. Hänggi, T.J. Mroczkowski, F. Moss, et al., Bistability driven by colored noise: theory and experiment, Phys. Rev. A 32 (1) (1985) 695.
- [23] L. Fronzoni, P. Grigolini, P. Hänggi, et al., Bistable oscillator dynamics driven by nonwhite noise, Phys. Rev. A 33 (1986) 3320.
- [24] J. Liu, J. Cao, Y. Wang, et al., Asymmetric stochastic resonance in a bistable system driven by non-gaussian colored noise, Physica A 517 (2019) 321-336.
- [25] P. Hänggi, P. Jung, C. Zerbe, et al., Can colored noise improve stochastic resonance? J. Stat. Phys. 70 (1993) 25–47.
- [26] P. Hänggi, M.E. Inchiosa, D. Fogliatti, et al., Nonlinear stochastic resonance: the saga of anomalous output-input gain, Phys. Rev. E 62 (2000) 6155.
- [27] L. Gammaitoni, E. Menichella-Saetta, S. Santucci, et al., Periodically time-modulated bistable systems: stochastic resonance, Phys. Rev. A 40 (1989) 2114.
- [28] L. Gammaitoni, P. Hänggi, P. Jung, F. Marchesoni, Stochastic resonance, Rev. Mod. Phys. 70 (1998) 223.
- [29] R. Benzi, A. Sutera, A. Vulpiani, The mechanism of stochastic resonance, J. Phys. A 14 (1981) L453.
- [30] F. Moss, L.M. Ward, W.G. Sannita, Stochastic resonance and sensory information processing: a tutorial and review of application, Clin. Neurophysiol. 115 (2004) 267–281.
- [31] R. Mantegna, B. Spagnolo, Stochastic resonance in a tunnel diode in the presence of white or coloured noise, Il Nuovo Cimento D 17 (1995) 873-881.
- [32] F. Castro, M. Kuperman, M. Fuentes, et al., Experimental evidence of stochastic resonance without tuning due to non-Gaussian noises, Phys. Rev. E 64 (2001) 051105.
- [33] D. Zhu, M.J. Tudor, S.P. Beeby, Strategies for increasing the operating frequency range of vibration energy harvesters: a review, Meas. Sci. Technol. 21 (2009) 022001.
- [34] L. Tang, Y. Yang, C.K. Soh, Toward broadband vibration-based energy harvesting, J. Intell. Mater. Syst. Struct. 21 (2010) 1867-1897.
- [35] R. Masana, M.F. Daqaq, Response of duffing-type harvesters to band-limited noise, J. Sound Vib. 332 (2013) 6755-6767.
- [36] E. Perkins, B. Balachandran, Noise-enhanced response of nonlinear oscillators, Procedia IUTAM 5 (2012) 59–68.
- [37] V. Agarwal, X. Zheng, B. Balachandran, Influence of noise on frequency responses of softening duffing oscillators, Phys. Lett. A 382 (2018) 3355-3364.
- [38] V. Agarwal, J.A. Yorke, B. Balachandran, Noise-induced chaotic-attractor escape route, Nonlinear Dyn. 102 (2020) 863–876.
- [39] A. Alofi, G. Acar, B. Balachandran, Noise influenced response movement in coupled oscillator arrays with multi-stability, J. Sound Vib. 531 (2022) 116951.
- [40] V. Agarwal, B. Balachandran, Noise-assisted response steering for a rotor-stator system, J. Sound Vib. 523 (2022) 116683.
- [41] B. Balachandran, T. Breunung, G.D. Acar, et al., Dynamics of circular oscillator arrays subjected to noise, Nonlinear Dyn 108 (2022) 1-14.
- [42] B.J. Matkowsky, Z. Schuss, The exit problem for randomly perturbed dynamical systems, SIAM J. Appl. Math. 33 (1977) 365–382.
- [43] M.I. Freidlin, A.D. Wentzell, Random Perturbations of Dynamical Systems, Springer, 1998.
- [44] L.D. Lutes, S. Sarkani, Random Vibrations: Analysis of Structural and Mechanical Systems, Butterworth-Heinemann, 2004.
- [45] F. Hooge, T. Kleinpenning, L.K. Vandamme, Experimental studies on 1/f noise, Rep. Prog. Phys. 44 (1981) 479.
- [46] W.H. Press, Flicker noises in astronomy and elsewhere, Comments Astrophys. 7 (1978) 103-119.
- [47] T. Musha, M. Yamamoto, 1/f fluctuations in biological systems, in: Proceedings of the 19th Annual International Conference of the IEEE Engineering in Medicine and Biology Society, vol. 6, IEEE, 1997, pp. 2692–2697.
- [48] K. Numata, A. Kemery, J. Camp, Thermal-noise limit in the frequency stabilization of lasers with rigid cavities, Phys. Rev. Lett. 93 (2004) 250602.
- [49] International Organization for Standardization, Mechanical vibration road surface profiles reporting of measured data, ISO 8608 (2016).
- [50] P. Múčka, Road waviness and the dynamic tyre force, Int. J. Veh. Des. 36 (2004) 216-232.
- [51] K.M. Cuddington, P. Yodzis, Black noise and population persistence, Proc. R. Soc. Lond. Ser. B 266 (1999) 969–973.
- [52] M. Schroeder, Fractals, Chaos, Power Laws: Minutes from an Infinite Paradise, Courier Corporation, 2009.
   [53] B.B. Mandelbrot, J.R. Wallis, Some long-run properties of geophysical records, Water Resour. Res. 5 (1969) 321–340.
- [54] S.H. Crandall, W.D. Mark, Random Vibration in Mechanical Systems, Academic Press, 2014.
- [55] F. Moon, P.J. Holmes, A magnetoelastic strange attractor, J. Sound Vib. 65 (1979) 275–296.
- [56] A.H. Nayfeh, D.T. Mook, Nonlinear Oscillations, John Wiley & Sons, 2008.

JID: TAML [m5G;January 21, 2023;10:15]

T. Breunung and B. Balachandran

Theoretical and Applied Mechanics Letters xxx (xxxx) xxx

- [57] G. Tomlinson, Force distortion in resonance testing of structures with electro-dynamic vibration exciters, J. Sound Vib. 63 (1979) 337–350.
- [58] H. Dankowicz, F. Schilder, Recipes for continuation, SIAM, 2013.
  [59] T. Breunung, B. Balachandran, Computationally efficient simulations of stochastically perturbed nonlinear dynamical systems, J. Comput. Nonlinear Dyn. 17 (2022) 091008, doi:10.1115/1.4054932
- [60] H. Hoffmann, Violin plot, 2022, https://www.mathworks.com/matlabcentral/fileexchange/45134-violin-plot MATLAB Central File Exchange., Retrieved: August 31, 2022.
- [61] D.C. Poirel, S.J. Price, Structurally nonlinear fluttering airfoil in turbulent flow, AIAA J. 39 (2001) 1960–1968.
  [62] N.E. Humphries, N. Queiroz, J.R. Dyer, et al., Environmental context explains Lévy and Brownian movement patterns of marine predators, Nature 465 (2010) 1066–1069.
  [63] D.W. Sims, E.J. Southall, N.E. Humphries, et al., Scaling laws of marine predator search behaviour, Nature 451 (2008) 1098–1102.
  [64] B.B. Mandelbrot, J.W. Van Ness, Fractional Brownian motions, fractional noises and applications, SIAM Rev. 10 (1968) 422–437.
  [65] R. Whittle, DSP generation of pink (1/f) noise, 2022, https://www.firstpr.com.au/dsp/pink-noise/#Filtering Accessed: 2022-09-22.